

Influence of Humidified Aerosol on Lidar Depolarization Measurements below Ice-Precipitating Arctic Stratus

BASTIAAN VAN DIEDENHOVEN

Center for Climate Systems Research, Columbia University, New York, New York

ANN M. FRIDLIND AND ANDREW S. ACKERMAN

NASA Goddard Institute for Space Studies, New York, New York

(Manuscript received 10 February 2010, in final form 23 May 2011)

ABSTRACT

Lidar measurements obtained during the Surface Heat Budget of the Arctic Ocean (SHEBA) experiment under a mixed-phase stratus cloud that was lightly precipitating ice show a range of surprisingly low depolarization ratios (4%–23%), despite an absence of cloud droplets there. These depolarization ratios are much lower than the range of theoretical values obtained for various ice habits. The depolarization ratios correlate well with radar reflectivity, suggesting that the variation in depolarization ratios results from variations in ice water content, rather than variation in ice habits or orientation. By calculating lidar depolarization based on (i) large-eddy simulations and (ii) in situ ice size distribution measurements, it is shown that the presence of humidified aerosol particles in addition to the ice precipitation can explain the distribution and vertical profile of the observed depolarization ratios, although uncertainties related to the aerosol size distributions are substantial. These calculations show that humidified aerosol must be taken into account when interpreting lidar depolarization measurements for cloud and precipitation phase discrimination or ice habit classification, at least under conditions similar to those observed during SHEBA.

1. Introduction

Lidar measurements can provide a wealth of information about macro- and microphysical properties of aerosols and clouds (Weitkamp 2005). In particular, lidars that emit circularly or linearly polarized light and measure the depolarization of the returned signal have proven to be very useful in the study of clouds. For instance, lidar depolarization measurements can be used to study and classify ice crystals in clouds and precipitation, since depolarization properties depend on microphysical properties of the ice crystals such as habit, aspect ratio, and crystal orientation (Noel et al. 2002; Del Guasta et al. 2006; You et al. 2006). Depolarization measurements can also be used to distinguish ice from liquid particles since light scattered from nonspherical ice particles is depolarized, whereas, in the absence of multiple scattering effects, light scattered from spherical drops is not

(Shupe et al. 2005; de Boer et al. 2011). Generally, linear depolarization ratios below about 10%–15% are considered to indicate liquid, while higher depolarizations point to the presence of ice crystals (Sassen et al. 1992; Intrieri et al. 2002). Some more advanced schemes use other measurements in addition to lidar depolarization to classify cloud phase, such as lidar backscatter coefficients, radar reflectivity, and Doppler velocity, but lidar depolarization serves as a critical parameter in these schemes (Shupe et al. 2005; Shupe 2007; Bourdages et al. 2009). In mixed-phase conditions, depolarization ratio measurements also can provide information about the relative concentrations of nonspherical ice and liquid drops (van Diedenhoven et al. 2009; Bourdages et al. 2009). For example, van Diedenhoven et al. (2009) evaluated simulations of a mixed-phase stratocumulus cloud observed during the Mixed-Phase Arctic Cloud Experiment (M-PACE; Verlinde et al. 2007) by comparing simulated and observed distributions of lidar backscatter, radar reflectivity, and radar Doppler velocity, in addition to distributions of circular depolarization ratios below cloud, measured to be between 0% and 200%

Corresponding author address: Bastiaan van Diedenhoven, 2880 Broadway, New York, NY 10025.
E-mail: bvandiedenhoven@giss.nasa.gov

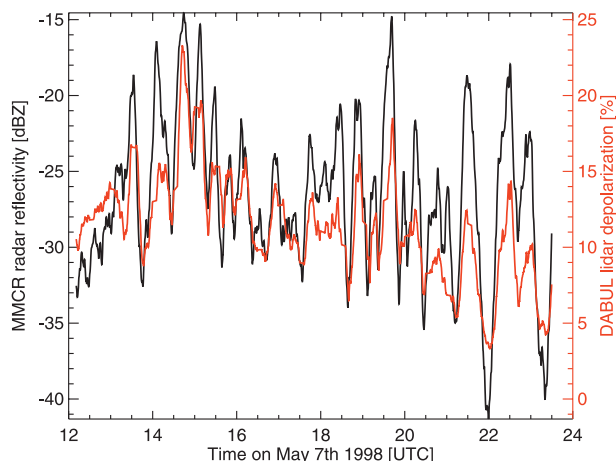


FIG. 1. The 10-min running means of MMCR radar reflectivity (black line, left axis) and lidar linear depolarization ratio (red line, right axis) measured during SHEBA in the last 12 h of 7 May 1998, averaged below cloud base (140–240 m) of a stratus layer.

(corresponding to linear depolarizations from 0% to ~50%; Mishchenko and Hovenier 1995). Only simulations with sufficiently rapid glaciation of mixed-phase precipitation (drizzle and ice) below cloud base were found to reproduce all radar and lidar metrics, including lidar depolarization. However, the impact of aerosol on depolarization was neglected in that study.

In this paper, we focus on linear depolarization measurements by the Depolarization and Backscatter Unattended Lidar (DABUL) under a mixed-phase stratus cloud observed during Surface Heat Budget of the Arctic Ocean (SHEBA) experiment (Uttal et al. 2002) over the last 12 h of 7 May 1998 (Zuidema et al. 2005). Figure 1 shows a time series of the 10-min running means of measured lidar depolarization below cloud base (140–240-m altitude). Measurements show linear depolarization ratios below cloud base ranging from 4% to 23%. Statistics presented by Intrieri et al. (2002) show that such low depolarization values were very commonly measured at low altitudes during the SHEBA campaign. These depolarization ratios are below the range of theoretical values associated with different ice habits, which typically vary from 25% to 70% (Sassen et al. 1992; Del Guasta et al. 2006; You et al. 2006), and are often below the limit of 10%–15% assumed to indicate liquid cloud particles. Furthermore, Fig. 1 shows that the depolarization ratios correlate well with the radar reflectivities under cloud measured by the Millimeter Cloud Radar (MMCR; Moran et al. 1998), with a linear correlation coefficient of 0.77. Considering radar reflectivity as a proxy for ice water content (Shupe et al. 2005), this correlation strongly suggests that changes in depolarization are associated with changes in ice water contents, rather than ice

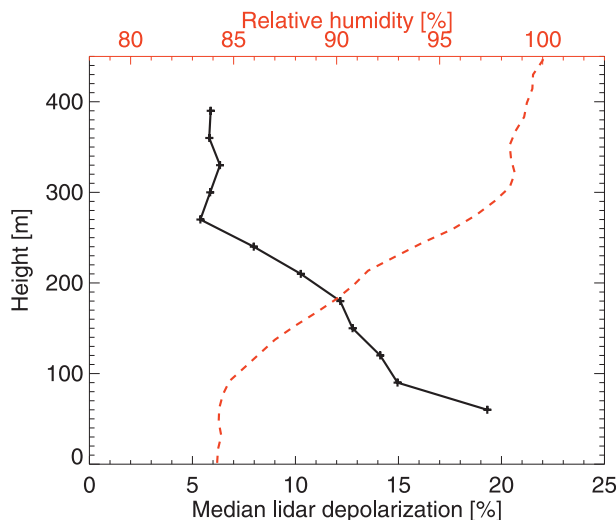


FIG. 2. Median depolarization values measured between 1200 and 0000 UTC as a function of height (black solid line, lower axis), and relative humidity measured by the 1800 UTC sounding (red dashed line, upper axis).

habit or aspect ratio variations or variations in ice orientation. However, as the observed cloud during SHEBA has a relatively low liquid water path and high droplet concentration, no liquid droplets are expected below cloud base (Comstock et al. 2004; Zuidema et al. 2005) to explain the low depolarization values in the regions with low ice concentrations. Also, in contrast to the M-PACE case study, no liquid precipitation was observed in cloud particle imager (CPI) images taken below cloud base (Zuidema et al. 2005). As hypothesized by Zuidema et al. (2005), these low depolarization values hint at the presence of humidified aerosol under cloud base. This hypothesis is supported by the observation that depolarization decreases with height, while relative humidity increases (Fig. 2). Also, it was noted previously by Sassen et al. (1992) that the vertical profile of lidar depolarization in the snowfall region below cloud base could be appreciably influenced by growing haze particles.

In this study we use calculations of depolarization ratios based on large-eddy simulations (LES) and in situ measurements to show that these low lidar depolarization ratios indeed can be explained by the presence of humidified aerosol particles amid ice precipitation, and that humidified aerosol should be considered when interpreting lidar depolarization measurements for cloud and precipitation phase discrimination and ice habit classification.

After describing the data in section 2 and simulations in section 3, we present results in section 4 and conclusions in section 5.

2. Measurements

As part of the SHEBA campaign, the DABUL lidar was deployed on an icebreaker ship frozen into the winter ice pack of the Beaufort Sea (Alvarez et al. 1998; Intrieri et al. 2002). DABUL operates at 532 μm and transmits linearly polarized light and measures the altitude-dependent linear depolarization ratio δ of the returned signal, defined as (Schotland et al. 1971)

$$\delta(z) = \frac{\beta_{\perp}(z)}{\beta_{\parallel}(z)} \exp(\tau_{\parallel} - \tau_{\perp}) \times 100\%, \quad (1)$$

where β and τ are the backscattering cross sections and atmospheric transmittances, respectively, in the planes of polarization perpendicular (\perp) and parallel (\parallel) to the laser's reference plane. Although DABUL was not well calibrated during SHEBA, calibration errors are expected to largely cancel out for the depolarization ratios, since the lidar uses a single detector to measure the backscatter in both polarization planes by alternating between polarization orientation for each pulse (Alvarez et al. 1998). As is general practice, we assume that the atmospheric transmission of light is largely independent of the polarization state, and the exponential term in Eq. (1) can be ignored (Schotland et al. 1971). The field of view of the DABUL measurements used here is 100 μrad , and its vertical and temporal resolutions are 30 m and 10 s, respectively. The lidar was tilted 5° off zenith to avoid specular reflection from oriented plates that result in depolarization values near zero (Intrieri et al. 2002).

The observed cloud base was steady around 280 m throughout the last 12 h UTC of 7 May 1998, while cloud-top height gradually fell from about 600 m at midday to around 400 m at the end of the day (Shupe et al. 2006; Fridlind et al. 2011). Cloud temperatures were roughly in the range from -16° to -20°C .

Unfortunately no aerosol size or composition measurements are available for SHEBA. Following Morrison et al. (2011), here we base the dry aerosol size distributions on those derived from measurements during M-PACE. Figure 3 shows particle concentrations measured in the five smallest size bins of the Met One Handheld Particle Counter (HHPC-6) flown on an Aerosonde unmanned aerial vehicle (UAV) on 10 October during M-PACE. Only HHPC-6 measurements below cloud base with an ambient relative humidity (RH) below 70% are considered here, since significant spurious high concentrations of particles in the largest bins are seen for higher RH. [For example, the interquartile range (IQR) of concentration in the 2–5- μm channel is 0.45 when all measurements are included and 0.09 when only measurements with $\text{RH} < 70\%$ are included.] Passing this

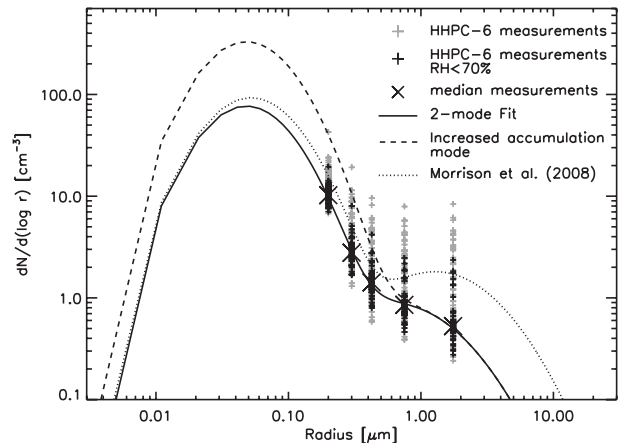


FIG. 3. HHPC-6 aerosol size distribution measurements taken during M-PACE, and the bimodal lognormal fit through median values (solid line). The dashed line shows the aerosol distribution with the number concentration increased in accumulation mode to represent polluted SHEBA conditions. The dotted line shows the fit of Morrison et al. (2008).

criteria are 41% of the HHPC-6 spectra. A six-parameter bimodal lognormal size distribution (geometric mean radius r_m , geometric standard deviation σ_g , and total number concentration N in each mode) was numerically fit through the median values of the HHPC-6 measurements (see the appendix and Fig. 3). To reflect the more polluted conditions during SHEBA relative to the M-PACE case, the number concentration in the fine mode was increased to 350 cm^{-3} , following Morrison et al. (2011). Figure 3 also includes the fit presented by Morrison et al. (2008), which differs significantly from ours, primarily in the coarse mode. This difference occurs mainly because Morrison et al. (2008) included HHPC-6 measurements at all RH and computed a fit through the mean values of the measurements as opposed to median values (the populations of counts within each channel are highly skewed). Morrison et al. (2008) focused their analysis on characterization of the fine mode, which is most important for constraining droplet activation, while characterization of the coarse mode is more important for lidar depolarization calculations since total scattering cross section is dominated by the coarse mode.

However, there is a substantial uncertainty associated with the derived aerosol size distributions. For example, the increase of number concentration in the accumulation mode for characterization of more polluted aerosol conditions during SHEBA is poorly constrained, although this mode only minimally contributes to the integrated cross-sectional area of the aerosol, which is the most important moment for our purposes. Furthermore, the range of integrated cross-sectional area of possible fits that fall within the IQR of the measurements in the five bins spans

more than a factor of 150 (see the appendix). Moreover, the SHEBA measurements were obtained over frozen ice pack, while the air mass sampled during M-PACE came from open ocean, probably leading to an increased coarse mode from sea salt. In light of the poorly constrained fit and to account for the expected absence of sea salt for the SHEBA conditions, we therefore also include lidar depolarization calculations based on the aerosol parameters with a decreased number concentration in the coarse mode. The derived aerosol characteristics for this case study are considered to be rough estimates, but sufficient to investigate the influence of humidified aerosol on lidar depolarization measurements.

In addition to lidar depolarization calculations based on LES, we also present lidar calculations based on in situ measured ice size distributions below cloud base. For this we use measurements obtained under cloud base between 2230 and 2300 UTC by the Forward Scattering Spectrometer Probe (FSSP; 0–53- μm maximum particle dimension) and two-dimensional cloud probe (2DC; $D > 62.5 \mu\text{m}$) mounted on the National Center for Atmospheric Research C-130 aircraft (Zuidema et al. 2005; Fridlind et al. 2011). Such measurements are known to suffer from ice crystal shattering on the probe tips, leading to a significant overestimation of number concentration especially for ice particles with a maximum dimension smaller than about 200 μm (Korolev and Isaac 2005; Korolev et al. 2011). To consider this effect, we also calculate lidar depolarization measurements based on the in situ size distribution in which crystals with a maximum dimension larger than 200 μm have been removed.

3. Simulations

The large-eddy simulations are made using the Distributed Hydrodynamic Aerosol-Radiation-Modeling Application (DHARMA) code (Stevens et al. 2002; Ackerman et al. 2003; Fridlind et al. 2011), which couples models of fluid dynamics, radiative transfer, and size-resolved, mixed-phase cloud microphysics. The DHARMA simulations represent the cloud observed in last two hours of the SHEBA case study as described in Fridlind et al. (2011), based in part on the SHEBA model intercomparison study (Morrison et al. 2011). The simulation domain is 1 km in depth and 3.2 km on a side with uniform respective grid mesh spacings of 10 and 50 m (results are not sensitive to using 5 and 25 m). A dynamical time step of 5 s is occasionally shortened to keep the advective Courant number below 0.8. The microphysical time step varies locally, depending upon the rate of processes occurring in a grid cell, to a minimum value of 0.2 s. Horizontal winds are nudged toward their initial

profiles with a 1-h time scale. To minimize errors associated with advection, the domain is translated with mean cloud-layer winds of 1.8 and 4.3 m s^{-1} from the west and south. Large-scale forcings, surface fluxes, aerosol, and ice nuclei (IN) are derived and applied as described in Fridlind et al. (2011). Liquid droplets and ice particles are tracked on a mass-doubling grid of 32 bins. Ice particle properties in each mass bin (maximum dimension, maximum projected area, and aspect ratio) are used to calculate fall speeds, collision-coalescence kernels, and vapor deposition and evaporation rates in an internally consistent manner based on the approach developed by Böhm (1999, 2004, and references contained therein). A combined analysis of in situ ice particle size distributions, cloud radar reflectivity and mean Doppler velocity measurements, and CPI data dictated the choice of radiating plates for ice of maximum dimension greater than 120 μm (see Fridlind et al. 2011). In the present study, we use a simulation described by Fridlind et al. (2011) that employs a prognostic approach to represent heterogeneous IN activation, thus accounting for IN sources, sinks, and transport (Fridlind et al. 2007), and with IN concentration increased by a factor of 30 relative to the IN measurements above cloud. We note that it has often been found that measured IN concentrations are insufficient to explain ice in mixed-phase clouds, although myriad uncertainties remain (Beard 1992; Fridlind et al. 2007; Morrison et al. 2008; Fan et al. 2009; van Diedenhoven et al. 2009). What is important for the purposes of this study is that the simulation used here reproduces average measured radar reflectivities and in situ measurements of ice crystal size distributions ($D > 200 \mu\text{m}$) quite well (Fridlind et al. 2011).

Since the model uses periodic boundary conditions, the position of the lidar does not correspond to any particular position in the horizontal plane of the model domain. To obtain statistics similar to those of the measurements, three time slices output during the last hour of the simulation are randomly sampled to obtain the same number of vertical columns (585) as in the measurements (cf. van Diedenhoven et al. 2009). Since the observed horizontal wind speeds are around 5 m s^{-1} (Fridlind et al. 2011), it takes on the order of 10 s for a parcel to advect across a 50-m-wide grid column. Since 10 s is also the time resolution of the lidar measurements, no averaging of model columns or lidar measurements is performed.

Lidar depolarization measurements are calculated from the DHARMA model results as described by van Diedenhoven et al. (2009), but for linearly rather than circularly polarized light. Furthermore, humidified aerosols are also included in the lidar calculations in the present study. Humidified aerosol particles are assumed to be spherical and therefore nondepolarizing. The scattering

properties for humidified aerosol are calculated using Lorenz–Mie theory (Weitkamp 2005). Scattering properties of the ice are calculated using the same assumptions of projected area and aspect ratio as made in the DHARMA microphysics treatment, which is described in more detail by Fridlind et al. (2011). In brief, the relation between projected area A_p and maximum dimension D corresponding to radiating assemblages of plates (Mitchell 1996) is assumed ($A_p = 0.2285D^{1.88}$ in cgs units). Using the mass–dimension relationships corresponding to this habit leads to the best agreement between measured radar reflectivities and the corresponding simulated values based on in situ measured ice size distributions; radiating assemblages of plates also agree well with CPI images obtained during the size distribution measurements (Fridlind et al. 2011). The aspect ratios are assumed to decrease linearly from 1.0 to 0.6 over a maximum dimension range of 5–120 μm , and to remain constant for larger sizes (cf. Korolev and Isaac 2003).

The optical properties are calculated using geometric optics (Macke et al. 1996), assuming the geometry of single, moderately roughened hexagonal plates with the projected areas and aspect ratios defined above. The ice crystals are assumed to be randomly oriented. Single hexagonal components of ice crystals have been shown to have similar optical properties as assemblages or aggregates of such components (e.g., Fu 2007; Um and McFarquhar 2009). Thus, the calculated optical properties are expected to represent the assumed assemblages of plates well. Depolarization ratios from backscattering off the assumed plates are about 40%, in agreement with values reported elsewhere (e.g., You et al. 2006; Noel et al. 2006; Yang and Fu 2009).

Radar reflectivities are simulated from the DHARMA model results using the Quickbeam package (Haynes et al. 2007) as described by van Diedenhoven et al. (2009).

Size distributions of the humidified aerosol are derived from the dry aerosol by numerically inverting the Köhler equation using the grid-scale relative humidities produced by the DHARMA model, and assuming a constant total number concentration of aerosol below cloud base, consistent with a well-mixed boundary layer aerosol. The aerosol is assumed to be ammonium bisulfate (Leck et al. 2002).

4. Results

Histograms of measured and simulated lidar depolarization under cloud base (60–120 m) for the last 2 h of the 7 May SHEBA case are shown in Fig. 4. Measured median depolarization is 9.4%, with an interquartile range of 7.8%. As expected, when no aerosol is included in the lidar simulations, calculated median depolarizations

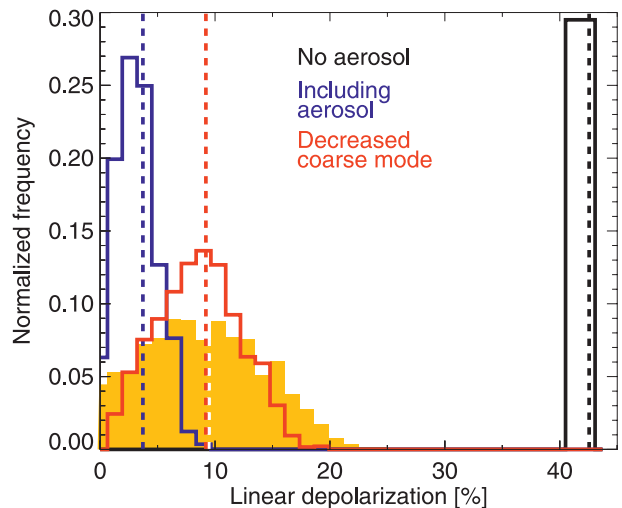


FIG. 4. Histograms of measured lidar depolarization ratios over 2200–0000 UTC (yellow), and those calculated based on the LES output, including no humidified aerosol (black), including all humidified aerosol (blue), and including humidified aerosol with the number concentration in the coarse mode decreased by a factor of 5 (red).

are much too high (42%). Adding an aerosol as specified by the fit obtained in section 2, the calculated depolarization values are too low with a median of 3.7% and an IQR of 2.5%. As discussed in section 2, the fit of aerosol parameters is not based on measurements obtained during SHEBA but rather is based on M-PACE measurements, and the concentrations of aerosol in the coarse mode, presumably dominated by sea salt, is expected to be significantly lower during SHEBA than during M-PACE. When we decrease the number concentration in the coarse mode by a factor of 5, the calculated depolarization histogram matches quite well with the observations as seen in Fig. 4, with a median value and IQR of 9.2% and 5.2%, respectively. Using scaling factors of 2 or 10 leads to median calculated depolarization values of 6.0% and 11.8%, respectively (not shown). As shown in Fig. 5, the observed vertical distribution of lidar depolarization below cloud base between 2200 and 0000 UTC is quite well matched by the simulations using the aerosol distribution with the coarse mode number concentration decreased by a factor of 5. Note that in the relatively optically thick cloud layer above 280 m the observed depolarization does not approach 0% owing to multiple scattering effects that are not included in our calculations. Figure 6 shows that the observed and simulated relations between radar reflectivity and lidar depolarization below cloud also agree well using the aerosol distribution with the coarse mode number concentration decreased by a factor of 5, although the observed reflectivities show a somewhat larger spread.

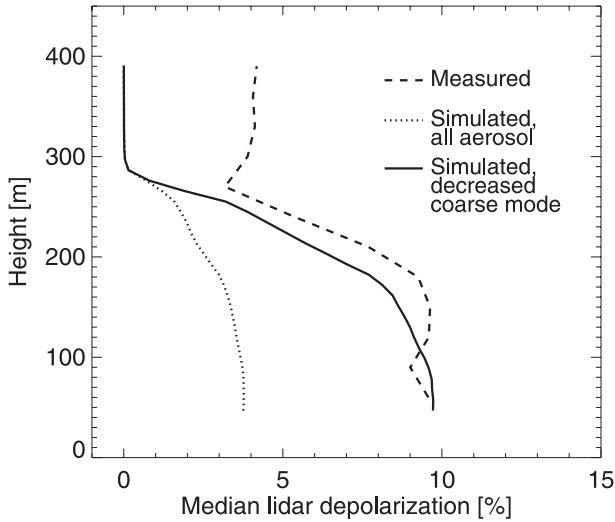


FIG. 5. Median depolarization values measured between 2200 and 0000 UTC as a function of height (dashed), and the corresponding simulated depolarization profiles including all humidified aerosol (dotted), and including humidified aerosol with the number concentration in the coarse mode decreased by a factor of 5 (solid).

When all aerosol is included in the calculations, the median radar reflectivities for a given lidar depolarization are about 5–10 dBZ higher. Extrapolating the simulated and observed relationships between radar reflectivity and lidar depolarization below cloud toward higher radar reflectivities leads to an estimation that lidar depolarization below cloud base reaches values around 40% (representative of ice crystals without the influence of aerosol) only when reflectivity values approach -10 dBZ. This suggests that lidar depolarization could be significantly influenced by humidified aerosols up to reflectivity values of about -10 dBZ under condition similar to those during SHEBA, and possibly up to 0 dBZ when more coarse mode aerosol is present.

The foregoing analysis is based on simulated ice size distributions. Figure 7 shows measured depolarization ratios (from 2230 to 2300 UTC) compared with those calculated based on the in situ measured (rather than simulated) size distributions, which are discussed in section 2. For this time span the measured median depolarization is 10%, with an interquartile range of 7.9%, similar to the measurements over 2200–0000 UTC. When the aerosol distribution with an unscaled coarse mode is included in the lidar calculations, the simulated depolarization ratios compare favorably to the measurements. However, as discussed in section 2, the measured concentration of small ice particles ($D < 200 \mu\text{m}$) likely suffers from ice shattering artifacts. Removing all ice with $D < 200 \mu\text{m}$ leads to depolarization ratios that are too low, with a median of 3.9%. When in addition the aerosol coarse mode number concentrations are decreased by a

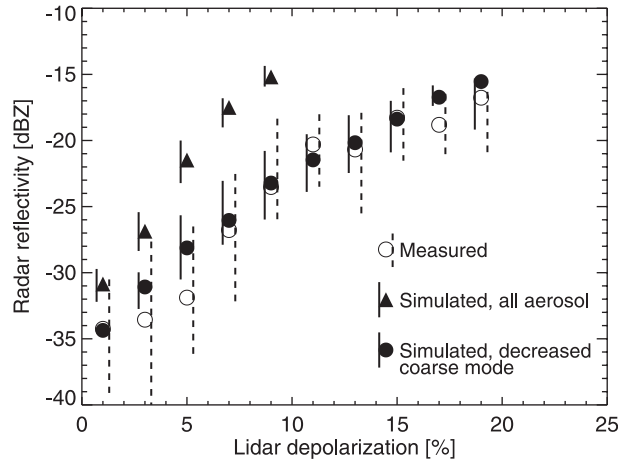


FIG. 6. Median and IQR of radar reflectivities within 2% depolarization bins measured between 2200 and 0000 UTC (open circles and dashed lines, respectively), and modeled including all humidified aerosol (triangles and solid lines, respectively), and humidified aerosol with the number concentration in the coarse mode decreased by a factor of 5 (closed circles and solid lines, respectively). Values are averaged over 140–240-m altitude.

factor of 5, the shape of the calculated depolarization distribution as well as its median and IQR of 9.8% and 7.8% respectively, again compare favorably with the measurements, and are similar to those calculated using the LES output. Removing all ice with $D < 150 \mu\text{m}$ or $D < 250 \mu\text{m}$, instead of $D < 200 \mu\text{m}$, leads to very similar results (not shown). Aside, we note that removing ice

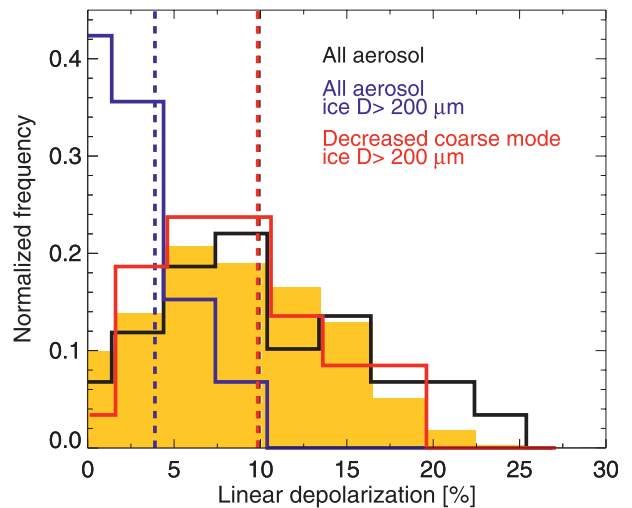


FIG. 7. Histograms of measured lidar depolarization ratios over 2230–2300 UTC (yellow), and those calculated based on the in situ measured ice size distributions, when all humidified aerosol and all ice are included (black), when all humidified aerosol and only large ice are included (blue), and when only large ice and humidified aerosol with the number concentration in the coarse mode decreased by a factor of 5 are included (red).

crystals with maximum dimension smaller than $200\ \mu\text{m}$ in the depolarization calculations based on LES output has a negligible effect (not shown), since very few small ice crystals are found below cloud base in these simulations (Fridlind et al. 2011).

These results show that the low lidar depolarization values and its vertical profile can be explained by the presence of ice precipitation and humidified aerosol under cloud base, and that aerosol effects may not generally be negligible under similar conditions, as is often assumed (e.g., Intrieri et al. 2002; van Diedenhoven et al. 2009; de Boer et al. 2011). In van Diedenhoven et al. (2009), we studied an M-PACE case of stratocumulus that was precipitating both ice and drizzle (median reflectivity of approximately 0 dBZ), and we attributed low lidar depolarization below cloud base primarily to the drizzle rather than humidified aerosol. Given that a well-mixed aerosol profile is able to reasonably explain the vertical profile of depolarization and the correlation between radar reflectivity and lidar depolarization in this SHEBA case without drizzle, future work should consider whether evaporating drizzle can generate a contrasting impact on depolarization below cloud base.

5. Conclusions

Using simulated lidar measurements based on (i) LES with size-resolved microphysics and (ii) in situ ice size distribution measurements, we investigate whether the presence of humidified aerosol can explain the surprisingly low linear depolarization ratios (4%–23%) measured below cloud base of an Arctic stratus deck during the SHEBA campaign. Aerosol size distribution measurements are not available for this SHEBA case study, so we follow Morrison et al. (2011) and derive a rough estimate of the aerosol size distribution from aerosol characteristics measured during M-PACE. We show that including this aerosol in the lidar calculations leads to an underestimation of the simulated lidar depolarization not only based on LES results but also on in situ ice size distributions with small ice crystals ($D < 200\ \mu\text{m}$) removed to crudely account for ice-shattering effects. Taking into account the fact that SHEBA measurements were obtained above a solid ice pack, while the aerosol size distributions were from marine air sampled during M-PACE, we also perform lidar depolarization calculations based on the aerosol parameters with a decreased number concentration in the coarse mode. When the aerosol coarse mode number concentrations are decreased by a factor of 5, the median and IQR of the measured lidar depolarization ratios are very well reproduced by the calculations based on LES output as well as on in situ measured ice size distributions. Also

the observed decrease of depolarization with height and the observed relationship between radar reflectivity and lidar depolarization are matched well by the calculations based on LES output including aerosol with the scaled coarse mode.

The uncertainties of the simulated lidar variables presented here are substantial, especially owing to uncertainties in the aerosol size distribution, but also because of limitations of the assumed ice optical properties, LES model assumptions, and in situ measured ice size distributions. Nevertheless, these results show that humidified aerosols should be taken into account when interpreting lidar depolarization measurements for cloud and precipitation phase discrimination or for ice habit classification, at least under conditions similar to those observed during SHEBA. We estimate that, under these conditions, aerosol could possibly have a significant effect on lidar depolarization for ice precipitation corresponding to radar reflectivities up to about $-10\ \text{dBZ}$. In situ aerosol size distribution measurements, coincident with improved ice size distribution measurements (expected to be available from future campaigns in the Arctic), should allow more rigorous investigations of humidified aerosol effects on the depolarization ratios measured under conditions similar to those explored here.

Acknowledgments. This work was supported by the National Aeronautics and Space Administration under Grant 06-EOS/06-100 issued through the Science Mission Directorate, Earth Science Division, and by the Department of Energy under Interagency Agreement DE-AI02-06ER64173 issued through the Office of Science, Office of Biological and Environmental Research. MMCR data were obtained from the Atmospheric Radiation Measurement (ARM) Program sponsored by the U.S. Department of Energy, Office of Science, Office of Biological and Environmental Research, Environmental Sciences Division. We thank Paquita Zuidema and Hugh Morisson for their help in obtaining the DABUL data and the in situ ice and aerosol size distribution data. Computational resources were provided by the DOE National Energy Research Scientific Computing Center, and by the NASA Advanced Supercomputing Division through the NASA High-End Computing Program. We thank two anonymous reviewers for their helpful comments and suggestions.

APPENDIX

Aerosol Size Distribution Fit

A six-parameter bimodal lognormal size distribution was fit to aerosol particle concentrations measured by

TABLE A1. Parameters of the bimodal lognormal fit to aerosol measurements.

Parameter	Fit range	Step size	Fit
$r_{m,1}$ (μm)	0.04–0.08	0.004	0.048
$\sigma_{g,1}$	1.5–2.5	0.1	2.0
N_1 (cm^{-3})	30–100	7.0	58*
$r_{m,2}$ (μm)	0.5–1.2	0.07	0.64
$\sigma_{g,2}$	1.6–5.0	0.34	2.62
N_2 (cm^{-3})	0.5–1.5	0.1	0.9

* Increased to 350 cm^{-3} to represent more polluted conditions during SHEBA.

the HHP-6 in five size bins. The parameters are geometric mean radius $r_{m,i}$, geometric standard deviation $\sigma_{g,i}$, and total number concentration N_i , in the accumulation mode ($i = 1$) and coarse mode ($i = 2$). With five bins and six parameters this fit is underconstrained. To obtain a reasonable fit to the measurements we vary the six parameters within the ranges and with the step sizes specified in Table A1. The combination of parameters that leads to the lowest RMS relative to the medians of the measurements is selected as the best fit shown in Fig. 3. We note that this fit poorly constrains the integrated cross-sectional area of the aerosol, which is important for our purpose. For example, using the method described above to find all possible fits that fall within the IQR of the measurements in the five bins, the range of derived integrated cross-sectional areas of these fits spans more than a factor of 150. The derived aerosol characteristics for this case study should be considered only as rough estimates.

REFERENCES

- Ackerman, A. S., O. B. Toon, D. E. Stevens, and J. A. Coakley Jr., 2003: Enhancement of cloud cover and suppression of nocturnal drizzle in stratocumulus polluted by haze. *Geophys. Res. Lett.*, **30**, 1381, doi:10.1029/2002GL016634.
- Alvarez, R. J., W. L. Eberhard, J. M. Intrieri, S. P. Sandberg, and K. W. Koenig, 1998: Cloud backscatter and phase measurements in the Arctic using ETL's DABUL lidar. *Proc. Fourth Int. Symp. on Tropospheric Profiling*, Snowmass, CO, CIRES, 7–9.
- Beard, K. V., 1992: Ice initiation in warm-base convective clouds: An assessment of microphysical mechanisms. *Atmos. Res.*, **28**, 125–152.
- Böhm, J. P., 1999: Revision and clarification of 'A general hydrodynamic theory for mixed-phase microphysics.' *Atmos. Res.*, **52** (3), 167–176.
- , 2004: Reply to comment on "Revision and clarification of 'A general hydrodynamic theory for mixed-phase microphysics' [Böhm J. P., 1999, Atmos. Res. 52, 167–176]." *Atmos. Res.*, **69**, 289–293.
- Bourdages, L., T. J. Duck, G. Lesins, J. R. Drummond, and E. W. Eloranta, 2009: Physical properties of high Arctic tropospheric particles during winter. *Atmos. Chem. Phys.*, **9**, 6881–6897.
- Comstock, K. K., R. Wood, S. E. Yuter, and C. S. Bretherton, 2004: Reflectivity and rain rate in and below drizzling stratocumulus. *Quart. J. Roy. Meteor. Soc.*, **130**, 2891–2918, doi:10.1256/qj.03.187.
- de Boer, G., H. Morrison, M. D. Shupe, and R. Hildner, 2011: Evidence of liquid dependent ice nucleation in high-latitude stratiform clouds from surface remote sensors. *Geophys. Res. Lett.*, **38**, L01803, doi:10.1029/2010GL046016.
- Del Guasta, M., E. Vallar, O. Riviere, F. Castagnoli, V. Venturi, and M. Morandi, 2006: Use of polarimetric lidar for the study of oriented ice plates in clouds. *Appl. Opt.*, **45**, 4878–4887.
- Fan, J., M. Ovtchinnikov, J. M. Comstock, S. A. McFarlane, and A. Khain, 2009: Ice formation in Arctic mixed-phase clouds: Insights from a 3-D cloud-resolving model with size-resolved aerosol and cloud microphysics. *J. Geophys. Res.*, **114**, D04205, doi:10.1029/2008JD010782.
- Fridlind, A. M., A. S. Ackerman, G. M. McFarquhar, G. Zhang, M. Poellot, P. DeMott, A. Prenni, and A. Heymsfield, 2007: Ice properties of single-layer stratocumulus during the Mixed-Phase Arctic Cloud Experiment: 2. Model results. *J. Geophys. Res.*, **112**, D24202, doi:10.1029/2007JD008646.
- , B. van Dierenhoven, A. S. Ackerman, A. Avramov, A. Mrowiec, H. Morrison, P. Zuidema, and M. D. Shupe, 2011: A FIRE-ACE/SHEBA case study of mixed-phase Arctic boundary-layer clouds. Entrainment rate limitations on rapid primary ice nucleation processes. *J. Atmos. Sci.*, in press.
- Fu, Q., 2007: A new parameterization of an asymmetry factor of cirrus clouds for climate models. *J. Atmos. Sci.*, **64**, 4140–4150.
- Haynes, J. M., R. T. Marchand, Z. Luo, A. Bodas-Salcedo, and G. L. Stephens, 2007: A multipurpose radar simulation package: QuickBeam. *Bull. Amer. Meteor. Soc.*, **88**, 1723–1727.
- Intrieri, J., M. Shupe, T. Uttal, and B. McCarty, 2002: An annual cycle of Arctic cloud characteristics observed by radar and lidar at SHEBA. *J. Geophys. Res.*, **107**, 8030, doi:10.1029/2000JC000423.
- Korolev, A., and G. A. Isaac, 2003: Roundness and aspect ratio of particles in ice clouds. *J. Atmos. Sci.*, **60**, 1795–1808.
- , and —, 2005: Shattering during sampling by OAPs and HVPS. Part I: Snow particles. *J. Atmos. Oceanic Technol.*, **22**, 528–542.
- , E. F. Emery, J. W. Strapp, S. G. Cober, G. A. Isaac, M. Wasey, and D. Marcotte, 2011: Small ice particles in tropospheric clouds: Fact or artifact? Airborne Icing Instrumentation Evaluation Experiment. *Bull. Amer. Meteor. Soc.*, **92**, 967–973.
- Leck, C., M. Norman, E. K. Bigg, and R. Hillamo, 2002: Chemical composition and sources of the high Arctic aerosol relevant for cloud formation. *J. Geophys. Res.*, **107**, 4135, doi:10.1029/2001JD001463.
- Macke, A., J. Mueller, and E. Raschke, 1996: Single scattering properties of atmospheric ice crystals. *J. Atmos. Sci.*, **53**, 2813–2825.
- Mishchenko, M. I., and J. W. Hovenier, 1995: Depolarization of light backscattered by randomly oriented nonspherical particles. *Opt. Lett.*, **20**, 1356–1358.
- Mitchell, D. L., 1996: Use of mass- and area-dimensional power laws for determining precipitation particle terminal velocities. *J. Atmos. Sci.*, **53**, 1710–1723.
- Moran, K. P., B. E. Martner, M. J. Post, R. A. Kropfli, D. C. Welsh, and K. B. Widener, 1998: An unattended cloud-profiling radar for use in climate research. *Bull. Amer. Meteor. Soc.*, **79**, 443–455.
- Morrison, H., J. O. Pinto, J. A. Curry, and G. M. McFarquhar, 2008: Sensitivity of modeled Arctic mixed-phase stratocumulus to cloud condensation and ice nuclei over regionally varying surface conditions. *J. Geophys. Res.*, **113**, D05203, doi:10.1029/2007JD008729.

- , and Coauthors, 2011: Intercomparison of cloud model simulations of arctic mixed-phase boundary layer clouds observed during SHEBA/FIRE-ACE. *J. Adv. Model. Earth Syst.*, **3**, M06003, doi:10.1029/2011MS000066.
- Noel, V., H. Chepfer, G. Ledanois, A. Delaval, and P. H. Flamant, 2002: Classification of particle effective shape ratios in cirrus clouds based on the lidar depolarization ratio. *Appl. Opt.*, **41**, 4245–4257, doi:10.1364/AO.41.004245.
- , —, M. Haeffelin, and Y. Morille, 2006: Classification of ice crystal shapes in midlatitude ice clouds from three years of lidar observations over the SIRTa observatory. *J. Atmos. Sci.*, **63**, 2978–2991.
- Sassen, K., H. Zhao, and G. C. Dodd, 1992: Simulated polarization diversity lidar returns from water and precipitating mixed phase clouds. *Appl. Opt.*, **31**, 2914–2923.
- Schotland, R. M., K. Sassen, and R. Stone, 1971: Observations by lidar of linear depolarization ratios for hydrometeors. *J. Appl. Meteor.*, **10**, 1011–1017.
- Shupe, M. D., 2007: A ground-based multisensor cloud phase classifier. *Geophys. Res. Lett.*, **34**, L22809, doi:10.1029/2007GL031008.
- , T. Uttal, and S. Y. Matrosov, 2005: Arctic cloud microphysics retrievals from surface-based remote sensors at SHEBA. *J. Appl. Meteor.*, **44**, 1544–1562.
- , S. Y. Matrosov, and T. Uttal, 2006: Arctic mixed-phase cloud properties derived from surface-based sensors at SHEBA. *J. Atmos. Sci.*, **63**, 697–711.
- Stevens, D. E., A. S. Ackerman, and C. S. Bretherton, 2002: Effects of domain size and numerical resolution on the simulation of shallow cumulus convection. *J. Atmos. Sci.*, **59**, 3285–3301.
- Um, J., and G. M. McFarquhar, 2009: Single-scattering properties of aggregates of plates. *Quart. J. Roy. Meteor. Soc.*, **135**, 291–304, doi:10.1002/qj.378.
- Uttal, T., and Coauthors, 2002: Surface heat budget of the arctic ocean. *Bull. Amer. Meteor. Soc.*, **83**, 255–275.
- van Diedenhoven, B., A. M. Fridlind, A. S. Ackerman, E. W. Eloranta, and G. M. McFarquhar, 2009: An evaluation of ice formation in large-eddy simulations of supercooled Arctic stratocumulus using ground-based lidar and cloud radar. *J. Geophys. Res.*, **114**, D10203, doi:10.1029/2008JD011198.
- Verlinde, J., and Coauthors, 2007: The Mixed-Phase Arctic Cloud Experiment. *Bull. Amer. Meteor. Soc.*, **88**, 205–221.
- Weitkamp, C., Ed., 2005: *Lidar: Range-Resolved Optical Remote Sensing of the Atmosphere*. Springer, 480 pp.
- Yang, P., and Q. Fu, 2009: Dependence of ice crystal optical properties on particle aspect ratio. *J. Quant. Spectrosc. Radiat. Transfer*, **110**, 1604–1614.
- You, Y., G. W. Kattawar, P. Yang, Y. X. Hu, and B. A. Baum, 2006: Sensitivity of depolarized lidar signals to cloud and aerosol particle properties. *J. Quant. Spectrosc. Radiat. Transfer*, **100**, 470–482, doi:10.1016/j.jqsrt.2005.11.058.
- Zuidema, P., and Coauthors, 2005: An Arctic springtime mixed-phase cloudy boundary layer observed during SHEBA. *J. Atmos. Sci.*, **62**, 160–176.